J. Fluid Mech. (2015), *vol.* 784, R5, doi:10.1017/jfm.2015.610

JFM RAPIDS
journals.cambridge.org/rapids

Enhanced heat transport in partitioned thermal convection

Yun Bao[1,2], Jun Chen[1], Bo-Fang Liu[3], Zhen-Su She[1], Jun Zhang[4,5] and Quan Zhou[3,†]

[1]State Key Laboratory for Turbulence and Complex Systems and Department of Mechanics and Engineering Science, College of Engineering, Peking University, Beijing 100871, China

[2]Department of Mechanics, Sun Yat-Sen University, Guangzhou 510275, China

[3]Shanghai Institute of Applied Mathematics and Mechanics and Shanghai Key Laboratory of Mechanics in Energy Engineering, Shanghai University, Shanghai 200072, China

[4]Courant Institute and Department of Physics, New York University, New York, NY 10012, USA

[5]NYU-ECNU Institutes of Mathematical Sciences and Physics Research, NYU-Shanghai, Shanghai 200062, China

(Received 29 August 2015; revised 14 October 2015; accepted 17 October 2015; first published online 6 November 2015)

Enhancement of heat transport across a fluid layer is of fundamental interest as well as great technological importance. For decades, Rayleigh–Bénard convection has been a paradigm for the study of convective heat transport, and how to improve its overall heat-transfer efficiency is still an open question. Here, we report an experimental and numerical study that reveals a novel mechanism that leads to much enhanced heat transport. When vertical partitions are inserted into a convection cell with thin gaps left open between the partition walls and the cooling/heating plates, it is found that the convective flow becomes self-organized and more coherent, leading to an unprecedented heat-transport enhancement. In particular, our experiments show that with six partition walls inserted, the heat flux can be increased by approximately 30 %. Numerical simulations show a remarkable heat-flux enhancement of up to 2.3 times (with 28 partition walls) that without any partitions.

Key words: Bénard convection, turbulent convection, turbulent flows

1. Introduction

Thermal convection is an efficient means to carry heat flux across space by a moving fluid, and it is ubiquitous in nature. A classical model system to study this phenomenon is Rayleigh–Bénard convection (RBC) (Ahlers, Grossmann & Lohse 2009; Lohse & Xia 2010), i.e. a thermally driven fluid layer lies above a horizontal

† Email address for correspondence: qzhou@shu.edu.cn

heating plate and below a cooling plate. Due to the buoyancy instability, the fluid moves and carries a heat flux upwards, which is typically many times that by thermal diffusion. An important question to ask is how much heat flux moves through the RBC cell given an enclosed fluid and an imposed temperature difference across the cell (Ahlers *et al.* 2009; Chillà & Schumacher 2012). This heat flux can be characterized by a non-dimensional parameter, defined as the Nusselt number

$$Nu = QH/\chi\Delta T, \tag{1.1}$$

which depends largely on the control parameters of the system, called the Rayleigh number and the Prandtl number, i.e.

$$Ra = \alpha g H^3 \Delta T/\nu\kappa \quad \text{and} \quad Pr = \nu/\kappa. \tag{1.2a,b}$$

Here, Q is the resulting heat flux across the fluid layer of thickness H for an applied temperature difference ΔT, g is the acceleration due to gravitation, and α, ν, κ and χ are respectively the thermal expansion coefficient, kinematic viscosity, thermal diffusivity and thermal conductivity of the enclosed fluid. The dependence of Nu on Ra and Pr has been extensively studied, both experimentally and numerically, in great detail for many years (Chavanne *et al.* 1997; Ashkenazi & Steinberg 1999; Grossmann & Lohse 2000; Kerr & Herring 2000; Niemela *et al.* 2000; Ahlers & Xu 2001; Xia, Lam & Zhou 2002; Verzicco & Camussi 2003; Roche *et al.* 2005; Gibert *et al.* 2009; du Puits, Resagk & Thess 2010; Silano, Sreenivasan & Verzicco 2010; Stevens, Lohse & Verzicco 2011; He *et al.* 2012; Urban *et al.* 2012; Huang & Zhou 2013; Wagner & Shishkina 2013). Scaling relationships were found from these studies, suggesting that a heat flux is determined once the Rayleigh and Prandtl numbers are known. For more detailed elucidation of the problem, we refer interested readers to the recent review papers by Ahlers *et al.* (2009) and Chillà & Schumacher (2012).

Another important problem that has been carefully investigated is to find out ways to enhance heat transport through RBC, which is particularly useful in many industrial processes and is of fundamental interest. Methods have been proposed to achieve high heat flux in modified RBC systems, such as by creating roughness on the conducting plates (Du & Tong 1998), imposing pulsed heating power on the lower plate (Jin & Xia 2008), rotating the convection cell about a vertical axis (King *et al.* 2009; Zhong *et al.* 2009*b*), employing multiphase working fluids (Zhong, Funfschilling & Ahlers 2009*a*; Biferale *et al.* 2012; Lakkaraju *et al.* 2013) and performing lateral confinement of the turbulent flows (Huang *et al.* 2013). In this paper, we present, both experimentally and numerically, a novel and yet simple method that significantly enhances heat transfer. In particular, our experiments show that by inserting several vertical partition walls into the convection cell, the heat transport can be increased by approximately 30 % (with six partition walls). Numerical simulations further show a dramatic heat-flux enhancement of up to 2.3 times (with 28 partition walls) that without any partitions. Below, we elaborate our experimental and numerical studies and reveal the mechanism of this enhancement of heat transfer.

The remainder of this paper is organized as follows. We give a brief description of the experimental set-up and the numerical method in § 2. Section 3 presents and analyses the heat-transport enhancement in partitioned RBC cells and reveals its mechanism. We summarize our findings and conclude in § 4.

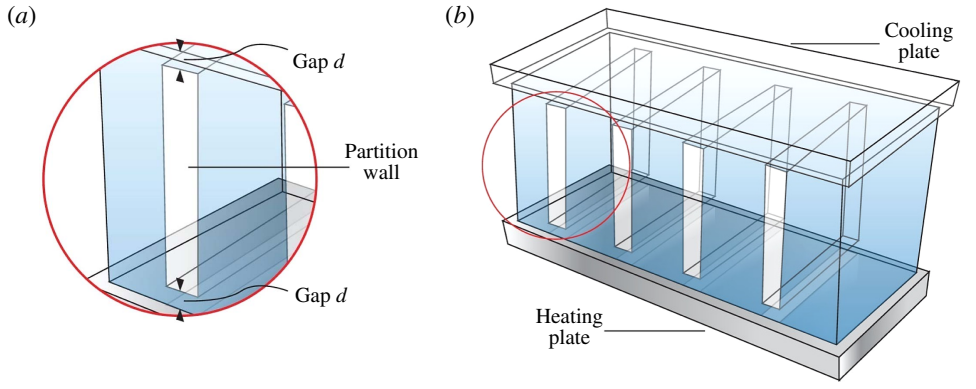

FIGURE 1. Schematic representation of the convection cell with four partition walls, dividing the original cell into five subcells (not in actual proportion). There are gaps of height d left open between the partition walls and the upper/lower conducting plates of the cell, allowing the subcells to communicate with each other.

2. Methods

2.1. *Experimental set-up*

Our experiments were carried out in a rectangular cell (Zhou *et al.* 2012, 2013), which measured $50 \times 15 \times 10$ (cm^3) in length (L), width (W) and height (H). The upper and lower thermally conducting plates were made of pure copper and their fluid-contact surfaces were electroplated with a thin layer of nickel to prevent oxidation by water. The sidewall was composed of four transparent Plexiglas plates of 1.2 cm thickness. As schematically shown in figure 1, several Plexiglas partition walls of 1.2 cm thickness were vertically inserted into the convection cell, equally spaced along the long side of the cell and parallel to its short side, thus dividing the RBC system into several equal-sized subcells. In order to allow the subcells to communicate with each other, we left gaps of 2 mm in height open between the partition walls and the horizontal plates. Without these gaps, the subcells would have been independent RBC systems that had different aspect ratios from the system without partitions, which have been studied extensively (Ahlers *et al.* 2009; Chillà & Schumacher 2012).

The temperature of the upper plate was regulated by passing cold water through its internal channels; the lower plate was heated at a constant power with two embedded film heaters. Thus, the experiments were conducted under constant-flux boundary conditions at the bottom plate while maintaining a constant temperature at the top plate. The temperature difference ΔT between the two plates was monitored by 12 thermistors; each plate had six, which were embedded uniformly across the plate. The working fluid was degassed water with a mean temperature of 31 °C, corresponding to a Prandtl number of $Pr = 5.3$, and the Nu measurements were made over a range of $3.5 \times 10^7 \lesssim Ra \lesssim 8.3 \times 10^8$. At each Ra, the system reached a well-developed state after 4–8 h, and our measurements were taken after an additional 12 h stabilization. A typical measurement of Nu lasted approximately 12 h. To reduce the influence of surrounding temperature fluctuations and minimize heat leakage, the entire RBC cell was wrapped in several layers of Styrofoam sheets and was placed in a thermostat throughout the measurements.

2.2. *Numerical methods*

The direct numerical simulations (DNS) were performed in several two-dimensional (2D) cells with increasing number of partitions ($n = 0$, 1, 2 and up to 35) at fixed Pr ($= 5.3$) and Ra ($= 1 \times 10^8$). Two considerations prompted us to focus on the 2D geometry. (i) The numerical effort required for 2D simulations is much smaller, so that a full resolution of the boundary layers (most active and crucial regions in RBC system) at high Rayleigh/Reynolds numbers is guaranteed and systematic studies can be performed. (ii) Detailed temperature and velocity fields are much easier to obtain in 2D. Such temperature and velocity information is readily available, so that complex physical mechanisms can be easily identified.

The numerical code is based on a finite-difference scheme of the incompressible Oberbeck–Boussinesq equations on a 2D domain of width $L = 50$ cm and height $H = 10$ cm. The equations are given by

$$\frac{\partial \boldsymbol{u}}{\partial t} + (\boldsymbol{u} \cdot \boldsymbol{\nabla})\boldsymbol{u} = -\boldsymbol{\nabla} p + \nu \nabla^2 \boldsymbol{u} + \alpha g T \boldsymbol{z}, \tag{2.1}$$

$$\boldsymbol{\nabla} \cdot \boldsymbol{u} = 0, \tag{2.2}$$

$$\frac{\partial T}{\partial t} + (\boldsymbol{u} \cdot \boldsymbol{\nabla}) T = \kappa \nabla^2 T, \tag{2.3}$$

for the velocity field $\boldsymbol{u}(\boldsymbol{x}, t)$, the kinematic pressure field $p(\boldsymbol{x}, t)$ and the temperature field $T(\boldsymbol{x}, t)$. Coordinates x and z are established along L and H respectively. Vertical partition walls of thickness 1.2 cm are inserted at equal horizontal spacing into the convection cell. Gaps of height d between the partition walls and the upper/lower conducting plates allow the fluid in each subcell to communicate with the fluid in other subcells. The velocity field obeys no-penetration and no-slip boundary conditions at all solid boundaries. The temperature field is isothermal at the top and bottom plates and adiabatic (no heat flux) at all other solid surfaces. To solve equations (2.1)–(2.3), we employed the idea of a projection algorithm (Chorin 1968). The space derivatives are approximated by the second-order central finite-difference scheme on a staggered grid (Harlow & Welch 1965). Due to the complicated computational situation induced by the solid boundaries of the partition walls, we employed the method of Gauss–Seidel iteration (see, e.g., Golub & van Loan 1996) to solve the Poisson equation for the pressure.

We briefly comment on the temporal and spatial resolutions. The time step was chosen to fulfil the Courant–Friedrichs–Lewy (CFL) condition, i.e. the CFL number was 0.2 or less for all of the simulations. The grid resolution was chosen to fully resolve the boundary layers (Shishkina *et al.* 2010) and the smallest scales in the bulk, i.e. the Kolmogorov scale η_K and the Batchelor scale η_B. In the present study, the number of grid points was set to 2000×450 for all runs. The horizontal grid size was equidistant but the vertical grid size was non-equidistant. Specifically, for all runs the gaps were resolved with 20 grid points in the vertical direction. For comparison and convergence purposes, simulations with the same parameters but 10 grid points within the gaps were also performed, which showed the agreement of the calculated Nu within 1 %. Thus, our choice of 20 grid points was proven to yield robust results.

In the present work, Nu was calculated over the whole volume and over time. The time convergence for the calculated Nu was checked by comparing the time averages over the first and the last halves of the simulations, and the resulting convergence was smaller than 1 % for all runs. We validated the numerical code by comparing our calculated Nu with previous results. To do this, we performed the simulation in

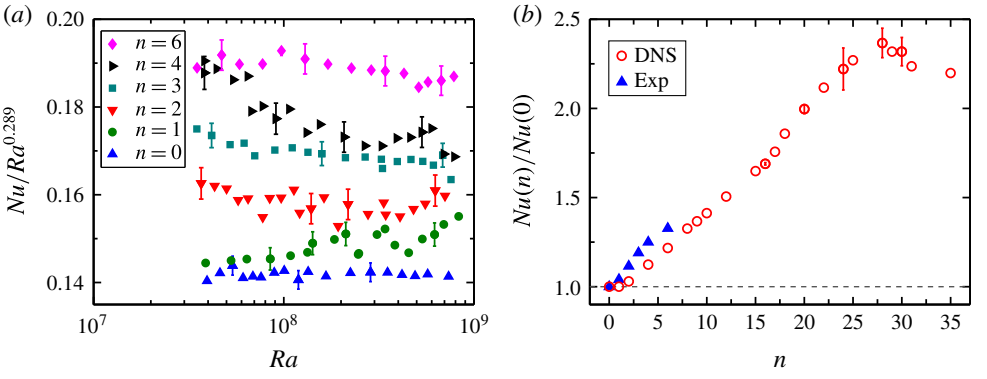

FIGURE 2. (*a*) Semi-log plot of $Nu/Ra^{0.289}$ as a function of Ra. Here, Nu is experimentally measured in rectangular cells with different numbers of partition walls, $n = 0$, 1, 2, 3, 4 and 6. The error bars shown in the figure reflect the fluctuating nature of thermal convection and finite measurement uncertainty. (*b*) Plot of $Nu(n)/Nu(0)$ as a function of the number of partition walls, n, at a gap height of $d = 2$ mm and $Ra = 1 \times 10^8$ from direct numerical simulations (DNS) (open circles) and experiments (solid triangles).

a 2D box of unit aspect ratio at $Ra = 1 \times 10^8$ and $Pr = 4.3$. The resulting Nusselt number we computed ($Nu = 25.85$) was in agreement with the one obtained for the same parameters by Sugiyama *et al.* (2009) and Zhou *et al.* (2011) ($Nu = 25.62$) to a precision of less than 1 %.

3. Results and discussion

Figure 2(*a*) shows a semi-log plot of the compensated Nusselt number, $Nu/Ra^{0.289}$, as a function of Ra. The measured values of Nu at $n = 0$ (no partitions) are the same as those measured in previous studies in the same parameter range (Zhou *et al.* 2012, 2013) and are described well by a power law Nu–$Ra^{0.289}$. As the number of partition walls increases from 0 to 6, however, Nu shows a clear monotonic increase. In particular, Nu is found to increase, on average, by ~4.3 %, 11.5 %, 19.0 %, 25.3 % and 32.7 % respectively for $n = 1$, 2, 3, 4 and 6. This is quite surprising and counterintuitive: now the more restricted convective flow by the partition walls does not impede the heat flux but rather enhances it. It should be noted that the thermal effects of the Plexiglas walls are negligible (Ahlers *et al.* 2009) and hence cannot account for the observed Nu enhancement. Furthermore, the power law fits to the measured Nu–Ra data yield scaling exponents in the range between 0.27 and 0.3. This exponent is consistent with those previously obtained in both rectangular (Zhou *et al.* 2012) and cylindrical cells (Funfschilling *et al.* 2005), suggesting that the present flow is still in the so-called 'classical' regime of turbulent RBC where the overall heat transfer of the system is dominated mainly by thermal boundary layers (Ahlers *et al.* 2009).

To gain insight into how the heat-transfer efficiency is improved by partition walls, we performed numerical studies in 2D cells at fixed Pr (= 5.3) and Ra (= 10^8) with different numbers of partitions. Figure 2(*b*) plots the obtained Nu as a function of the number of partition walls, n. Here, $Nu(n)$ is normalized by $Nu(n = 0)$ to show the enhancement effects. Both the 2D numerical and three-dimensional (3D) experimental results are plotted in the figure to show the heat-exchange enhancement. It is clear

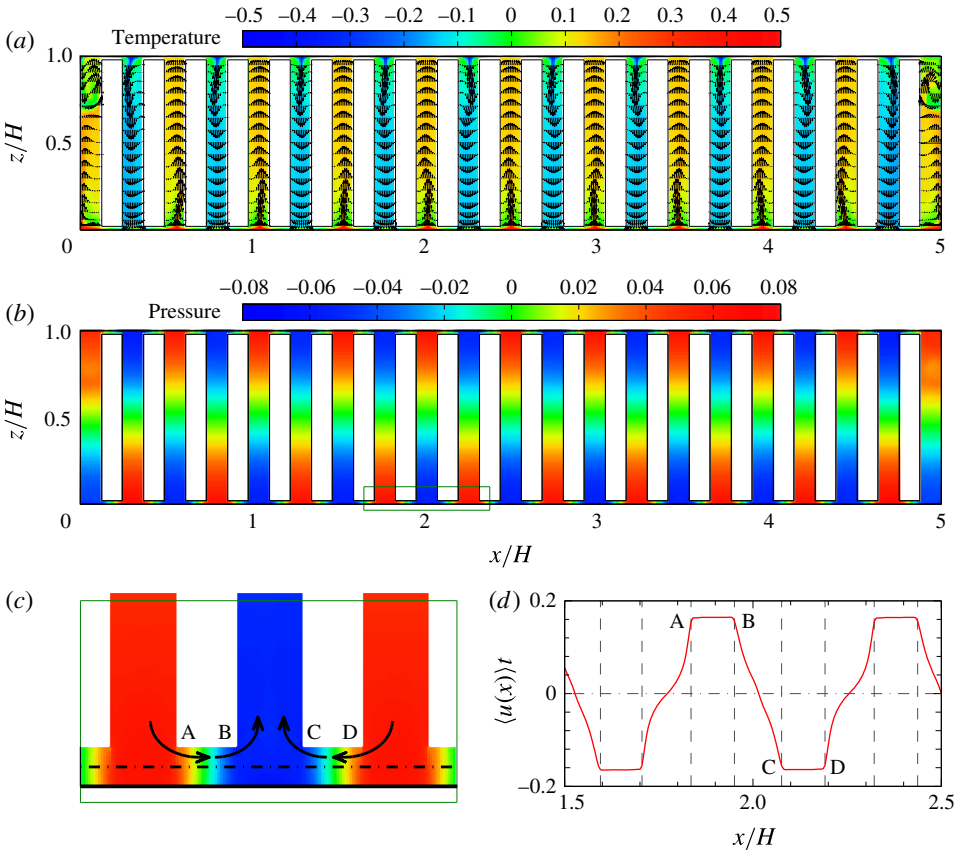

FIGURE 3. (*a*) Time-averaged non-dimensionalized temperature (colour) and velocity (arrows) fields obtained in a 2D numerical RBC cell with 20 partition walls at $d = 2$ mm and $Ra = 1 \times 10^8$. Here, the red and blue colours correspond to the high- and low-temperature regions respectively. (*b*) The corresponding time-averaged non-dimensionalized pressure field. (*c*) An enlarged portion of the pressure field, indicated by the dark-green box in (*b*), near the heated lower plate. The red and blue colours in (*b*) and (*c*) correspond to the high- and low-pressure regions respectively. (*d*) The corresponding mean horizontal velocity profile $\langle u(x)\rangle_t$ calculated at the mid-height of the thin gaps near the lower plate ($z = d/2$, indicted by the horizontal dash–dot line in (*c*)). The vertical dashed lines mark the positions of partition walls. Corresponding movies can be found in the supplementary material available at http://dx.doi.org/10.1017/jfm.2015.610.

that the 2D simulations yield similar results to the experiments for small numbers of partitions (up to six), and the trend of enhancement extends monotonically up to $n = 28$, where the heat flux is enhanced by 130 %. This amount of enhancement is unprecedented, indicating a promising technological potential once implemented in practice.

To reveal how this remarkable increase of heat flux is achieved, we looked closely into the flow structures inside the cells and their temperature and pressure distributions. Figure 3(*a*) shows the flow pattern in a system with 20 partition walls, and overlapped with the temperature field, where the local temperature is indicated according to the colour bar. Apparently, the system has undertaken a

symmetry-breaking bifurcation: the fluid in each subcell moves unidirectionally and takes on directions alternatively across partition walls. In particular, fluid in subcells with higher temperature moves upwards and cooler fluid moves downwards; velocity and temperature are precisely correlated. The fluid circulates between adjacent subcells through the gaps, ensuring fluid continuity. The symmetry-breaking bifurcation also leads to a pressure distribution that sustains the above coherent flow, as evidenced by figure 3(*b*). Here, one sees clearly that near both the top and bottom conducting plates the high- and low-pressure regions alternately appear at the two horizontal ends of the thin gaps. This is shown more clearly in a close-up plot in figure 3(*c*). Here, the pressure field is established by the buoyancy-driven flow, and subsequently drives the horizontal flows within the gaps. Figure 3(*d*) shows the time-averaged horizontal velocity profile $\langle u(x)\rangle_t$ computed at the mid-height of the thin gaps near the lower plate ($z/H = d/2$). The vertical dashed lines in the figure indicate the positions of partition walls. One sees that due to the horizontal pressure drop across each gap there is a strong horizontal jet within all thin gaps. This jet in the gaps sweeps the thermal boundary layers, brings the hot or cold fluid into the bulk of the subcells, and thus realizes the efficient heat exchange in the system. It should be noticed that our preliminary simulations in 3D geometry reveal similar results: when 28 partition walls are inserted into the system, the global heat flux can be enhanced by approximately 113 % and the observed flow structures – including the velocity, temperature and pressure fields – are similar to those of 2D simulations, as shown in figure 3.

The enhancement of the overall heat flux through the system is realized by two effects. First, the flows in each subcell become more coherent when the number of partition walls n is large, i.e. the mean velocity and temperature fields are strongly correlated with each other in each subcell, and hence carry a more effective heat flux. On the other hand, there is always a competing effect: as n increases, the heat-carrying fluid is reduced and the impedance from the partition walls increases, both of which reduce the overall heat transport. From these reasonings, one may expect that there should be an optimum number of partition walls; this is indeed observed in figure 2(*b*). The second factor is the existence of jet flows in the thin gaps that sweep the local boundary layers. In fact, some previous studies have taken the approach of inserting horizontal partitions into the system to obstruct and alter the convective flow pattern, but have found that the heat-transfer efficiency changes little (Ciliberto, Cioni & Laroche 1996; Xia & Lui 1997). This is because in the so-called classical regime heat transport is limited by the thickness of the thermal boundary layer, and altering the flow dynamics by these horizontal partitions has little effect on the boundary layers. In contrast, close inspection of our simulation data regarding the local temperature distribution in the thin gaps shows that the jet can effectively reduce the thermal boundary layer thickness to at most 1/3 of that of the traditional RBC system (no partitions) at the same Ra. Thus, the jet induces a large increase of the temperature gradient at the conducting plates, and hence the heat flux (e.g. Nu). This suggests that the strong horizontal jets in thin gaps are the main contributors to the heat-transfer enhancement. This mechanism highlights the importance of the gap height: at a gap height of the order of the thermal boundary layer, the maximum heat-transfer enhancement can be realized.

Figure 4 shows the normalized Nu as a function of the gap height d obtained in a 2D cell with six partition walls. Here, d is normalized by the thermal boundary layer thickness δ_{th} $[= H/2Nu(0)]$ obtained in the convection cell with no partitions. The figure shows that Nu reaches a maximum value as $d \sim \delta_{th}$. The physical mechanism

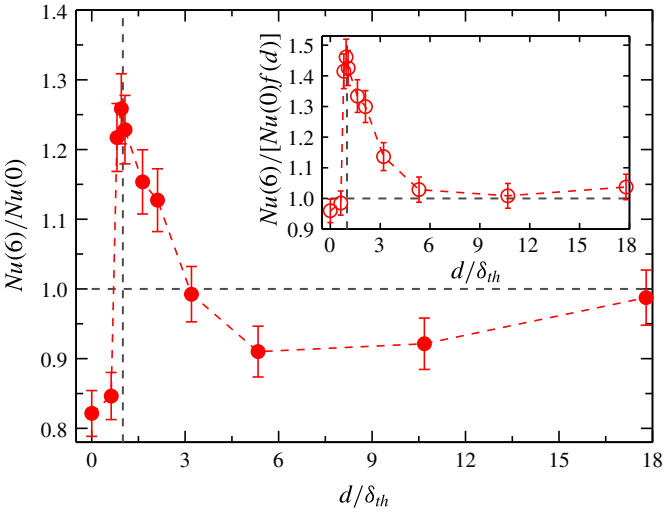

FIGURE 4. Plot of $Nu(6)/Nu(0)$ as a function of the normalized gap height d/δ_{th} from numerical simulations. The horizontal dashed line indicates $Nu(6)/Nu(0) = 1$ and the vertical dashed line marks the position $d = \delta_{th}$. One sees that the heat-transfer enhancement is optimized when $d \sim \delta_{th}$. Inset: the volume-corrected plot of $Nu(6)/[Nu(0)f(d)]$ as a function of d/δ_{th}, where $f(d)$ is the actual fluid volume normalized by the volume of the cell (when there are no partitions).

is similar to that found by Liu & Zhang (2008) in thermal convection, where the fluid interacts with many mobile spherical insulators. The thermal insulation is most effective when the radius of the insulators matches the thickness of the thermal boundary layer. From the flow visualizations, we find that the horizontal jet flow within the gaps reaches its highest intensity when the gap height d is comparable with δ_{th}. For too narrow gaps, an increased resistance within the gap restrains the flow within the gaps and thus reduces the overall heat transport, while for too large d there is no significant pressure-drop buildup so that the jet flow nearly vanishes. Furthermore, it is seen that $Nu(6)$ recovers to $Nu(0)$ for large d ($d = H/3 \approx 18\delta_{th}$), as the partition walls play little role in modifying the flows. On the other hand, for $d = 0$, the overall heat transport is reduced because of the vanished jets in the gaps and the limited heat-carrying fluid volume. If the decrease of the fluid volume is accounted for, as shown in the inset of figure 4 (the leftmost point), the Nusselt number is found to be the same as that of any non-communicating convection subcells.

4. Conclusion

In conclusion, a partitioned RBC system with thin gaps connecting neighbouring cells is able to produce a qualitatively different flow pattern that greatly enhances the heat flux. The most interesting phenomenon revealed by the present study is the observed symmetry-breaking bifurcation, which is similar to the self-organized formation of the convection roll in traditional RBC (Xi, Lam & Xia 2004). There, cold and hot plumes are entrained by the convection roll to two sides of the cell, forming a horizontal pressure gradient, which, in the present work, drives the jet flow in the thin gaps. Thus, the sustained circulations around the partition walls may be considered as a series of convection rolls with alternating and unidirectional flows in

each subcell. Moreover, our preliminary simulations suggest that the heat-transport enhancement can be further optimized by either varying the thickness of the partition walls or changing the aspect ratio of the convection cell; these effects will be investigated in a future study.

Acknowledgements

We thank B. Liu, H.-Y. Zou and Z.-X. Yin for helpful discussions. This work was financially supported by the Natural Science Foundation of China under grant nos. 11372362 (Y.B.), 11452002 (Z.-S.S. and J.C.), 11472106 (J.Z.), 11222222 and 11572185 (Q.Z.). Q.Z. wishes to acknowledge support given to him from Program for New Century Excellent Talents in University under grant no. NCET-13 and Shanghai Shuguang Project under grant no. 13SG40, the organization department of the CPC central committee through National Program for Support of Top-notch Young Professionals.

Supplementary movies

Supplementary movies are available at http://dx.doi.org/10.1017/jfm.2015.610.

References

AHLERS, G., GROSSMANN, S. & LOHSE, D. 2009 Heat transfer and large scale dynamics in turbulent Rayleigh–Bénard convection. *Rev. Mod. Phys.* **81**, 503–537.

AHLERS, G. & XU, X.-C. 2001 Prandtl-number dependence of heat transport in turbulent Rayleigh–Bénard convection. *Phys. Rev. Lett.* **86**, 3320–3323.

ASHKENAZI, S. & STEINBERG, V. 1999 High Rayleigh number turbulent convection in a gas near the gas–liquid critical point. *Phys. Rev. Lett.* **83**, 4760–4763.

BIFERALE, L., PERLEKAR, P., SBRAGAGLIA, M. & TOSCHI, F. 2012 Convection in multiphase fluid flows using lattice Boltzmann methods. *Phys. Rev. Lett.* **108**, 104502.

CHAVANNE, X., CHILLÀ, F., CASTAING, B., HEBRAL, B., CHABAUD, B. & CHAUSSY, J. 1997 Observation of the ultimate regime in Rayleigh–Bénard convection. *Phys. Rev. Lett.* **79**, 3648–3651.

CHILLÀ, F. & SCHUMACHER, J. 2012 New perspectives in turbulent Rayleigh–Bénard convection. *Eur. Phys. J.* E **35**, 58.

CHORIN, A. J. 1968 Numerical solution of the Navier–Stokes equations. *Maths. Comput.* **22** (104), 745–762.

CILIBERTO, S., CIONI, S. & LAROCHE, C. 1996 Large-scale flow properties of turbulent thermal convection. *Phys. Rev. Lett.* **54** (6), R5901–R5904.

DU, Y.-B. & TONG, P. 1998 Enhanced heat transport in turbulent convection over a rough surface. *Phys. Rev. Lett.* **81**, 987–990.

FUNFSCHILLING, D., BROWN, E., NIKOLAENKO, A. & AHLERS, G. 2005 Heat transport by turbulent Rayleigh–Bénard convection in cylindrical samples with aspect ratio one and larger. *J. Fluid Mech.* **536**, 145–154.

GIBERT, M., PABIOU, H., TISSERAND, J.-C., GERTJERENKEN, B., CASTAING, B. & CHILLÀ, F. 2009 Heat convection in a vertical channel: plumes versus turbulent diffusion. *Phys. Fluids* **21**, 035109.

GOLUB, G. H. & VAN LOAN, C. F. 1996 *Matrix Computations*, 3rd edn. Johns Hopkins.

GROSSMANN, S. & LOHSE, D. 2000 Scaling in thermal convection: a unifying theory. *J. Fluid Mech.* **407**, 27–56.

HARLOW, F. H. & WELCH, J. E. 1965 Numerical calculation of time-dependent viscous incompressible flow of fluid with free surface. *Phys. Fluids* **8**, 2182–2189.

HE, X.-Z., FUNFSCHILLING, D., NOBACH, H., BODENSCHATZ, E. & AHLERS, G. 2012 Transition to the ultimate state of turbulent Rayleigh–Bénard convection. *Phys. Rev. Lett.* **108**, 024502.

HUANG, S.-D., KACZOROWSKI, M., NI, R. & XIA, K.-Q. 2013 Confinement-induced heat transport enhancement in turbulent thermal convection. *Phys. Rev. Lett.* **111**, 104501.

HUANG, Y.-X. & ZHOU, Q. 2013 Counter-gradient heat transport in two-dimensional turbulent Rayleigh–Bénard convection. *J. Fluid Mech.* **737**, R3.

JIN, X.-L. & XIA, K.-Q. 2008 An experimental study of kicked thermal turbulence. *J. Fluid Mech.* **606**, 133–151.

KERR, R. M. & HERRING, J. 2000 Prandtl number dependence of Nusselt number in direct numerical simulations. *J. Fluid Mech.* **491**, 325–344.

KING, E. M., STELLMACH, S., NOIR, J., HANSEN, U. & AURNOW, J. M. 2009 Boundary layer control of rotating convection systems. *Nature* **457**, 301–304.

LAKKARAJU, R., STEVENS, R. J. A. M., ORESTA, P., VERZICCO, R., LOHSE, D. & PROSPERETTI, A. 2013 Heat transport in bubbling turbulent Rayleigh–Bénard convection. *Proc. Natl Acad. Sci. USA* **110**, 9237–9242.

LIU, B. & ZHANG, J. 2008 Self-induced cyclic reorganization of many bodies through thermal convection. *Phys. Rev. Lett.* **100**, 244501.

LOHSE, D. & XIA, K.-Q. 2010 Small-scale properties of turbulent Rayleigh–Bénard convection. *Annu. Rev. Fluid Mech.* **42**, 335–364.

NIEMELA, J. J., SKRBEK, L., SREENIVASAN, K. R. & DONNELLY, R. J. 2000 Turbulent convection at very high Rayleigh numbers. *Nature* **404**, 837–840.

DU PUITS, R., RESAGK, C. & THESS, A. 2010 Measurements of the instantaneous local heat flux in turbulent Rayleigh–Bénard convection. *New J. Phys.* **12**, 075023.

ROCHE, P.-E., GAUTHIER, F., CHABAUD, B. & HÉBRAL, B. 2005 Ultimate regime of convection: robustness to poor thermal reservoirs. *Phys. Fluids* **17**, 115107.

SHISHKINA, O., STEVENS, R. J. A. M., GROSSMANN, S. & LOHSE, D. 2010 Boundary layer structure in turbulent thermal convection and its consequences for the required numerical resolution. *New J. Phys.* **12**, 075022.

SILANO, G., SREENIVASAN, K. R. & VERZICCO, R. 2010 Numerical simulations of Rayleigh–Bénard convection for Prandtl numbers between 10^{-1} and 10^4 and Rayleigh numbers between 10^5 and 10^9. *J. Fluid Mech.* **662**, 409–446.

STEVENS, R. J. A. M., LOHSE, D. & VERZICCO, R. 2011 Prandtl and Rayleigh number dependence of heat transport in high Rayleigh number thermal convection. *J. Fluid Mech.* **688**, 31–43.

SUGIYAMA, K., CALZAVARINI, E., GROSSMANN, S. & LOHSE, D. 2009 Flow organization in two-dimensional non-Oberbeck–Boussinesq Rayleigh–Bénard convection in water. *J. Fluid Mech.* **637**, 105–135.

URBAN, R., HANZELKA, P., KRALIK, T., MUSILOVA, V., SRNKA, A. & SKRBEK, L. 2012 Effect of boundary layers asymmetry on heat transfer efficiency in turbulent Rayleigh–Bénard convection at very high Rayleigh numbers. *Phys. Rev. Lett.* **109**, 154301.

VERZICCO, R. & CAMUSSI, R. 2003 Numerical experiments on strongly turbulent thermal convection in a slender cylindrical cell. *J. Fluid Mech.* **477**, 19–49.

WAGNER, C. & SHISHKINA, O. 2013 Aspect-ratio dependency of Rayleigh–Bénard convection in box-shaped containers. *Phys. Fluids* **25**, 085110.

XI, H.-D., LAM, S. & XIA, K.-Q. 2004 From laminar plumes to organized flows: the onset of large-scale circulation in turbulent thermal convection. *J. Fluid Mech.* **503**, 47–56.

XIA, K.-Q., LAM, S. & ZHOU, S.-Q. 2002 Heat-flux measurement in high-Prandtl-number turbulent Rayleigh–Bénard convection. *Phys. Rev. Lett.* **88**, 064501.

XIA, K.-Q. & LUI, S.-L. 1997 Turbulent thermal convection with an obstructed sidewall. *Phys. Rev. Lett.* **79**, 5006–5009.

ZHONG, J.-Q., FUNFSCHILLING, D. & AHLERS, G. 2009*a* Enhanced heat transport by turbulent two-phase Rayleigh–Bénard convection. *Phys. Rev. Lett.* **102**, 124501.

ZHONG, J.-Q., STEVENS, R. J. A. M., CLERCX, H. J. H., VERZICCO, R., LOHSE, D. & AHLERS, G. 2009*b* Prandtl-, Rayleigh-, and Rossby-number dependence of heat transport in turbulent rotating Rayleigh–Bénard convection. *Phys. Rev. Lett.* **102**, 044502.

ZHOU, Q., LIU, B.-F., LI, C.-M. & ZHONG, B.-C. 2012 Aspect ratio dependence of heat transport by turbulent Rayleigh–Bénard convection in rectangular cells. *J. Fluid Mech.* **710**, 260–276.

ZHOU, Q., LU, H., LIU, B.-F. & ZHONG, B.-C. 2013 Measurements of heat transport by turbulent Rayleigh–Bénard convection in rectangular cells of widely varying aspect ratios. *Sci. China-Phys. Mech. Astron.* **56**, 989–994.

ZHOU, Q., SUGIYAMA, K., STEVENS, R. J. A. M., GROSSMANN, S., LOHSE, D. & XIA, K.-Q. 2011 Horizontal structures of velocity and temperature boundary layers in two-dimensional numerical turbulent Rayleigh–Bénard convection. *Phys. Fluids* **23**, 125104.